Sensors and Materials, Vol. 38, No. 3 (2026) 1193–1205
MYU Tokyo

S & M 4371

CO_2/SF_6-based Deep Reactive Ion Etching of Si

Akihiro Matsutani,* Mina Sato, Miho Fujimoto, and Mie Tohnishi

Research Infrastructure Management Center, Institute of Science Tokyo,
4259 Nagatsuta-cho, Midori-ku, Yokohama 226-8501, Japan

(Received December 22, 2025; accepted February 5, 2026)

Keywords: deep-RIE, Si, CO_2, passivation, global warming potential

We demonstrated the vertical etching of Si by CO_2/SF_6-based deep reactive ion etching (deep-RIE) and investigated the dependence of the etching profile on the passivation process time, CO_2 flow rate, inductively coupled plasma (ICP) power, and process pressure. In addition, we demonstrated the microloading effect and investigated the fluorine resistance of the passivation film by XeF_2 vapor-phase etching. Furthermore, to investigate the composition of the sidewall passivation film, we performed the optical emission spectroscopy of the plasma during the deep-RIE and energy-dispersive X-ray and X-ray photoelectron spectroscopy analyses of the chemical composition of the passivation film on the etched Si sidewall. We found that the main components of the sidewall passivation film in CO_2/SF_6-based deep-RIE are C and O derived from the CO_2 plasma and Si oxides.

1. Introduction

Deep reactive ion etching (deep-RIE) is an effective microfabrication technique widely used in the fabrication of micro-electromechanical systems (MEMS).[1–9] In Si dry etching, a switching process called the Bosch process using C_4F_8/SF_6 plasma is widely used, as shown in Fig. 1(a).[10,11] In this process, a fluorocarbon-based passivation film is deposited on the etched surface and sidewalls using C_4F_8 plasma, as previously reported.[12–18] However, our previous study revealed that the main component of the passivation film on the sidewalls of narrow trenches is carbon, as shown in Fig. 1(b).[19] In conventional C_4F_8/SF_6-based deep-RIE, the global warming potential (GWP) of C_4F_8 used for passivation film formation is approximately 10,000. We have noticed that carbon films also function satisfactorily as passivation films, and we propose using CO_2, which has a GWP of 1 and is readily available, instead of C_4F_8 for the passivation process, as shown in Fig. 2. However, there have been only few reports to date on the demonstration and basic experiments of the vertical etching of Si by CO_2/SF_6-based deep-RIE.

In this study, we investigated the vertical etching of Si by CO_2/SF_6-based deep-RIE and the dependence of the etching profile on the passivation process time, CO_2 flow rate, inductively coupled plasma (ICP) power, and process pressure. In addition, we demonstrated the microloading effect and investigted the fluorine resistance of the passivation film by XeF_2

*Corresponding author: e-mail: matsutani.a.644e@m.isct.ac.jp
https://doi.org/10.18494/SAM6138

ISSN 0914-4935
https://myukk.org/

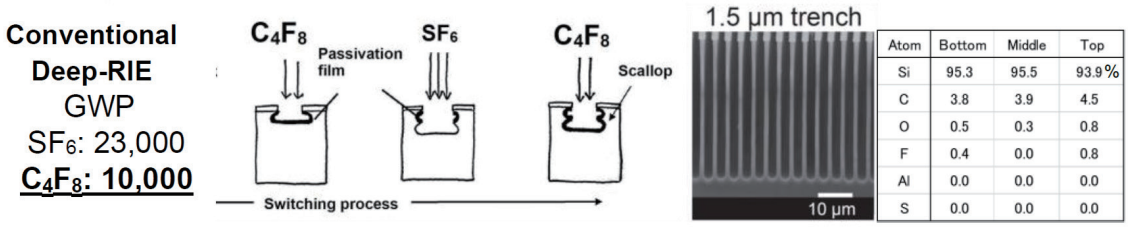

(a) (b)

Fig. 1. Conventional deep-RIE using SF_6/C_4F_8 plasma. (a) Schematic process and (b) etched trench structure and chemical composition of the etched sidewall.[19]

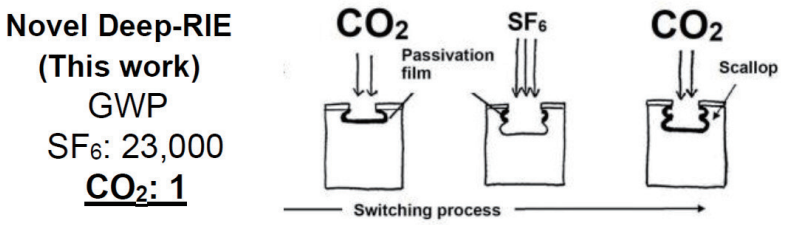

Fig. 2. Schematic of deep-RIE using SF_6/CO_2 plasma proposed in this study.

vapor-phase etching. To investigate the composition of the sidewall passivation film, we performed the optical emission spectroscopy of the plasma during the deep-RIE and energy-dispersive X-ray (EDX) and X-ray photoelectron spectroscopy (XPS) analyses of the chemical composition of the passivation film on the etched Si sidewall.

2. Experimental Setup of CO_2/SF_6-based deep-RIE

A deep-RIE system (SPP Technologies, MUC-21) was used for this experiment. As shown in Fig. 3, CO_2 was used for passivation and SF_6 for etching. These gases were introduced into the process chamber using mass flow controllers. CO_2 was supplied via a C_4F_8 mass flow controller. The actual flow rate must be converted by taking into account the conversion factor. The conversion factor for CO_2 is 0.75, whereas that for C_4F_8 is 0.17. Therefore, when CO_2 is supplied via a mass flow controller calibrated with C_4F_8, the actual CO_2 flow rate is 4.4 times the indicated flow rate. In this paper, the converted CO_2 flow rate is used. A 1.5 × 1.5 cm^2 Si substrate sample was placed on an aluminum sample tray of 200 mm diameter. An aluminum line-and-space pattern fabricated by photolithography using a contact aligner and sputter deposition was used as the etching mask. All deep-RIE processes in this paper were performed using a switching process, first forming a passivation film using CO_2 plasma and then etching with SF_6 plasma. Therefore, the deep-RIE begins with the passivation process and ends with the etching process. The passivation and etching processes were switched continuously. In other words, the parameters for each process were switched simultaneously. However, the actual gas exchange in the chamber involves a residence time due to the conductance of the exhaust system, so the switching is not completely discrete, and the two gases are mixed for a short period of time.

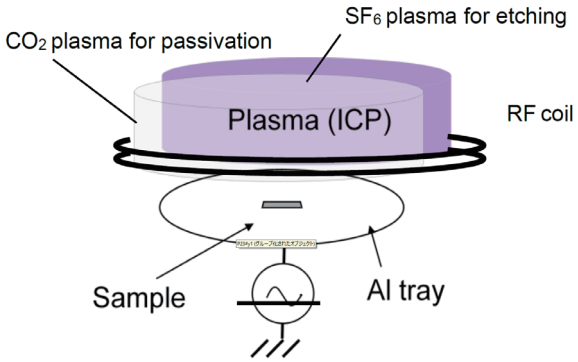

Fig. 3. (Color online) CO_2/SF_6-based deep-RIE system used in this experiment.

3. Experimental Results and Discussion

3.1 Time dependence of etching profile on passivation process

Figures 4(a)–4(d) show the experimental results of the time dependence of the etching profile on the passivation process. Figure 4(a) shows an etching profile obtained by continuous etching using only SF_6, not a switching process, with an etching time of 1 min. Because this etching process was performed using only SF_6, the etching profile is isotropic. The number of switching cycles for the etching profile and passivation process shown in Figs. 4(b)–4(d) was 55. CO_2 was supplied at a flow rate of 880 sccm. The SF_6 flow rate was 400 sccm. The etching process time for one cycle was 2.6 s. It can be seen that the passivation process time (i.e., the thickness of the passivation film) significantly contributes to the etching profile, and that a longer passivation process time results in less side etching and a more vertically etched profile. Therefore, it was found that the thickness of the passivation film is important for vertical etching. In the SEM image resolution, the verticality of the etching profile in the area where the passivation film was functioning, shown in Fig. 4(b), was approximately 90°. That of the etching profile shown in Figs. 4(c) and 4(d) was also approximately 90°.

Incidentally, the deposition rate of the passivation film formed continuously on the Si substrate surface using only CO_2 under the conditions of ICP/bias power of 1800/0 W and process pressure of 2 Pa was 26 nm/min. The etching rate for the results shown in Fig. 4(d) was 0.33 μm/cycle.

3.2 CO2 flow rate dependence

Figure 5(a) shows the dependence of etching depth on CO_2 flow rate. Figures 5(b)–5(d) show the dependence of etching profile on CO_2 flow rate. The etching conditions other than the CO_2 flow rate were as follows: for the passivation process, the ICP/bias power was 1800/0 W, the process pressure was 2 Pa, and the process time was 30 s; for the etching process, the SF_6 flow rate was 400 sccm, the ICP/bias power was 2300/40 W, the process pressure was 3 Pa, and the process time was 2.6 s. The passivation and etching processes were cycled 55 times. Figure 5(b)

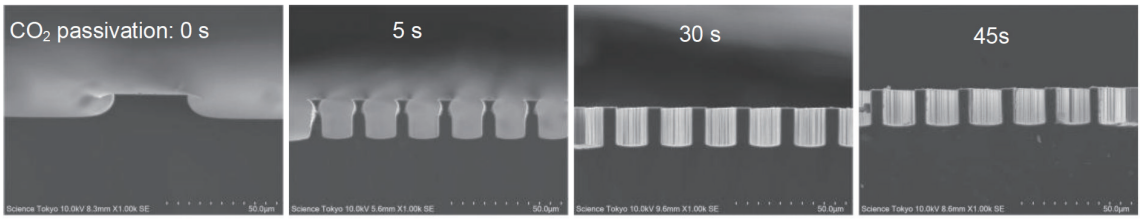

(a) (b) (c) (d)

Fig. 4. Time dependence of etching profile on passivation process.

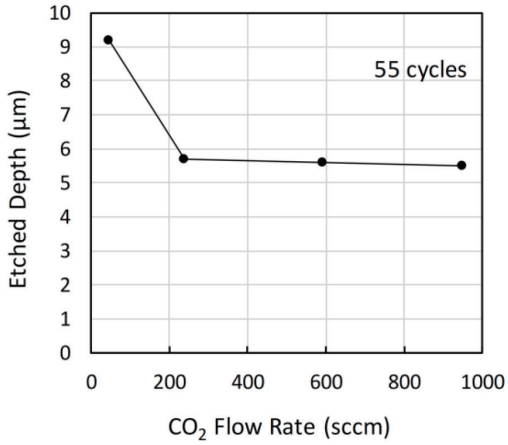

(a)

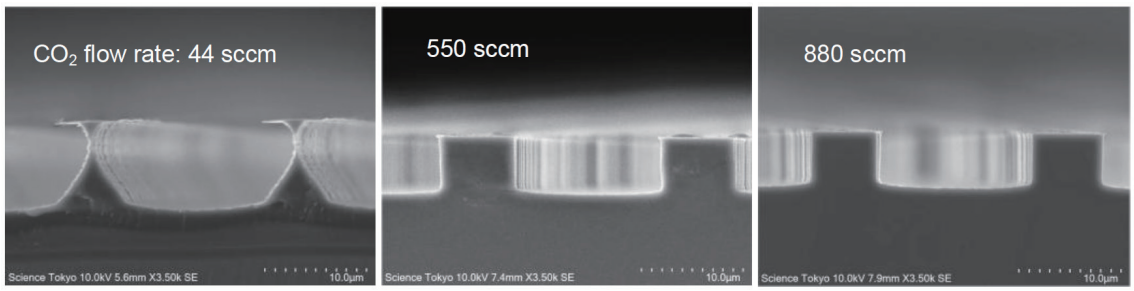

(b) (c) (d)

Fig. 5. Dependence of etching depth and profile on CO_2 flow rate.

shows the etching profile with significant side etching and undercutting, resulting in the largest etching depth. Figures 5(c) and 5(d) show vertical etching profiles with almost no undercutting and nearly identical etching depths. From these results, it is considered that in the passivation process, when the CO_2 flow rate is 44 sccm, the thickness of the passivation film on the etching sidewall is insufficient, and the effect of isotropic etching by SF_6 becomes dominant. On the other hand, when the CO_2 flow rate is 550 sccm or higher, the thickness of the passivation film on the etching sidewall is sufficient, and vertical fine processing can be achieved by the switching process combined with SF_6 etching.

3.3 ICP power dependence in passivation process

Figure 6(a) shows the ICP power dependence of etching depth during the passivation process. Figures 6(b)–6(d) show this dependence in the etching profile. The etching conditions other than the ICP power were as follows: bias power 0 W, CO_2 flow rate 880 sccm, process pressure 2 Pa, and process time 30 s for the passivation process; SF_6 flow rate 400 sccm, ICP/bias power 2300/40 W, process pressure 3 Pa, and process time 2.6 s for the etching process. The passivation and etching processes were cycled 55 times. Figure 6(b) shows significant side etching in the etching profile. Figure 6(c) shows slight side etching near the center of the etching depth, whereas Fig. 6(d) shows a vertical etching profile. In both cases, there was almost no undercutting, and the etching depth was nearly the same, as shown in Fig. 6(a). These results show that in the passivation process, an appropriate ICP power is required to ensure a passivation film thickness on the etching sidewalls sufficient for vertical etching.

3.4 Pressure dependence in passivation process

Figure 7(a) shows the pressure dependence of the etching depth during the passivation process. Figures 7(b)–7(d) show the pressure dependence of the etching profile. The etching

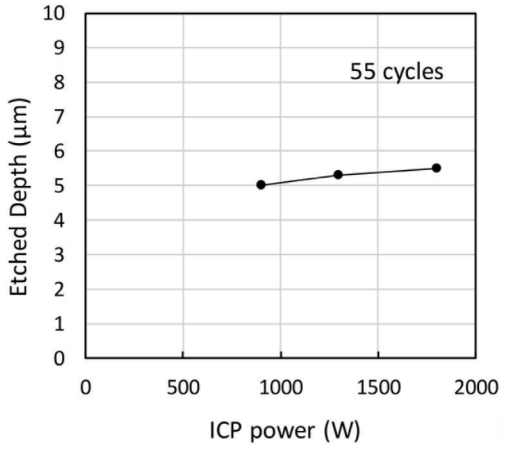

(a)

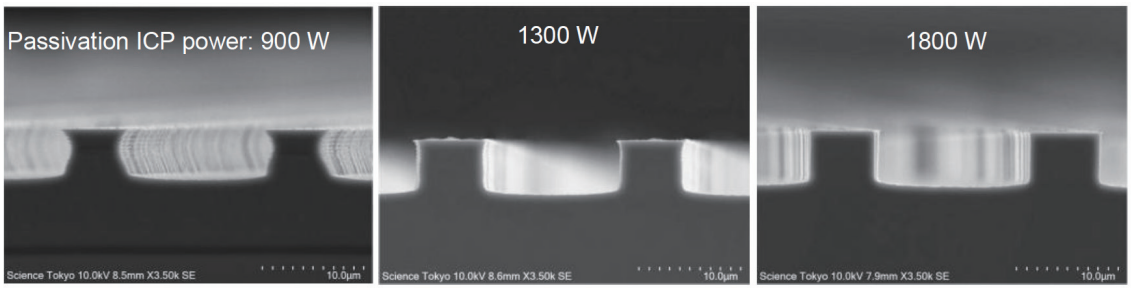

(b) (c) (d)

Fig. 6. Dependence of etching depth and profile on ICP power during passivation process.

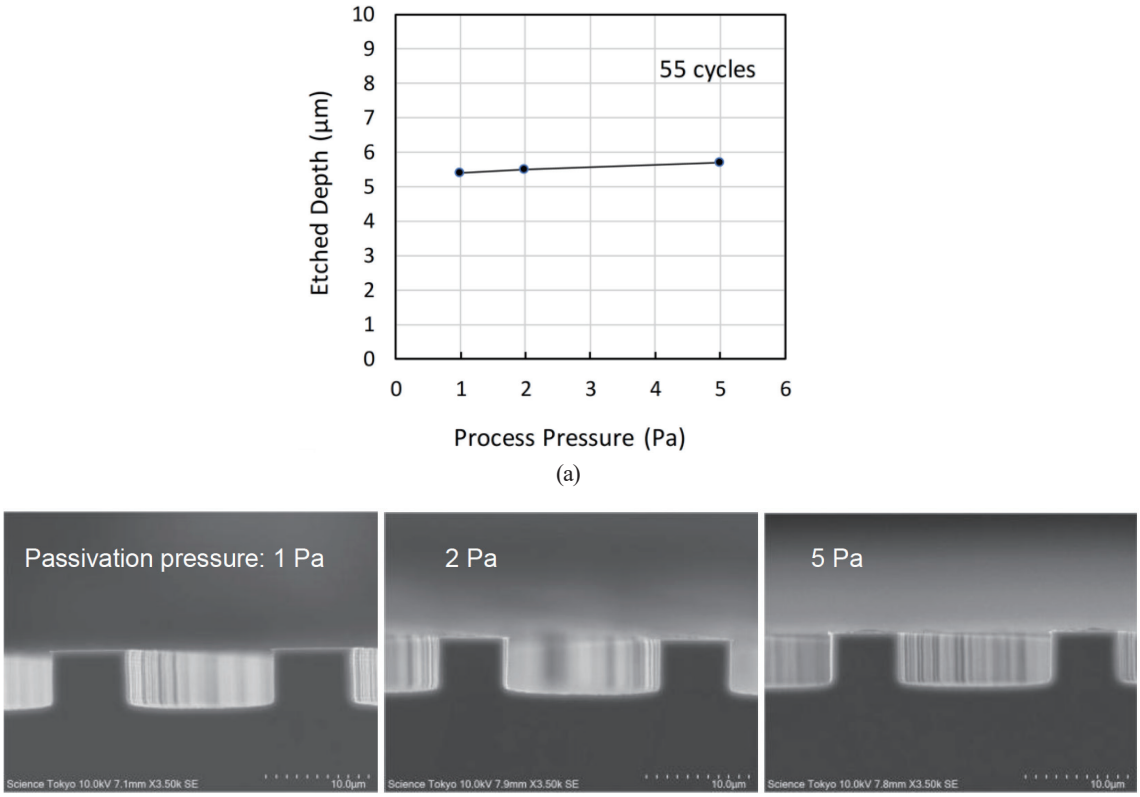

(a)

(b) (c) (d)

Fig. 7. Pressure dependence of etching depth and profile during passivation process.

conditions other than the pressure were as follows: for the passivation process, ICP/bias power 1800/0 W, CO_2 flow rate 880 sccm, and process time 30 s; for the etching process, SF_6 flow rate 400 sccm, ICP/bias power 2300/40 W, process pressure 3 Pa, and process time 2.6 s. The passivation and etching processes were cycled 55 times. In these figures, the etching profile showed no significant side etching, and the etching profile was vertical at all pressures. Furthermore, the etching depth was nearly the same at all pressures. These results show that in the passivation process, to ensure a passivation film thickness on the etching sidewalls sufficient for vertical etching, the process pressure is not the dominant parameter within the range of 1–5 Pa, and the process window is wide.

3.5 Microloading effect

We investigated the microloading effect in CO_2/SF_6-based deep-RIE. The experimental conditions for the passivation process were a CO_2 flow rate of 880 sccm, an ICP/bias power of 1800/0 W, a process pressure of 2 Pa, and a process time of 30 s. The etching process conditions were a SF_6 flow rate of 400 sccm, an ICP/bias power of 2300/40 W, a process pressure of 3 Pa, and a process time of 2.6 s. Fifty-five cycles of passivation and etching a processes were performed. Figure 8 shows the experimental results of the microloading effect. Similar to conventional plasma etching, a microloading effect was observed, where the etch depth

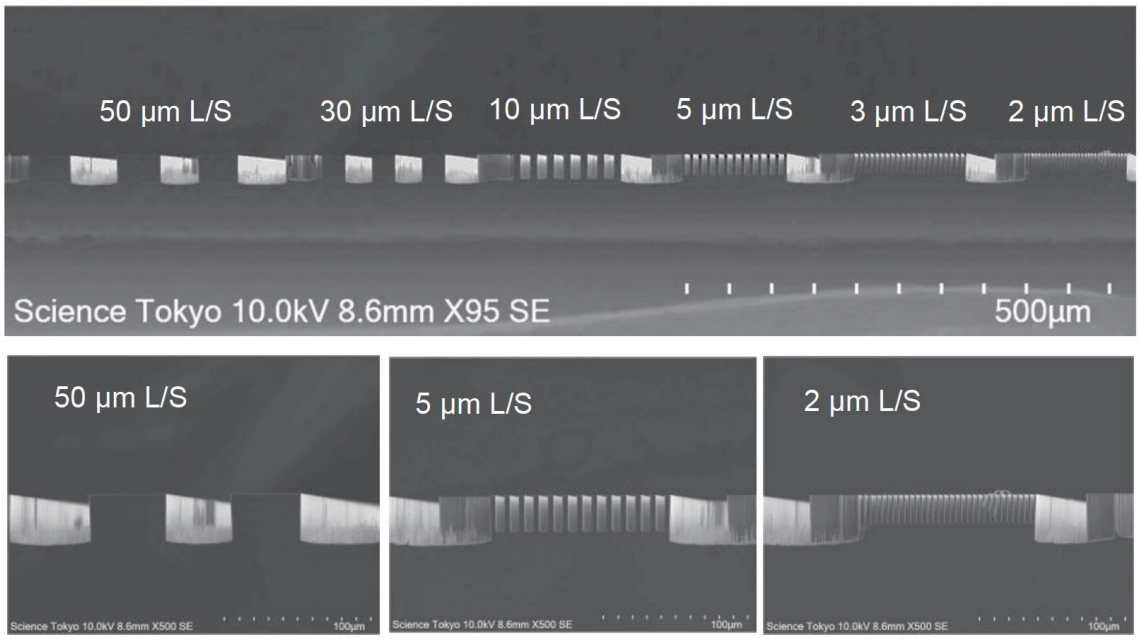

Fig. 8. Microloading effect in CO_2/SF_6-based deep-RIE.

decreased as the trench narrowed. This suggests that CO_2/SF_6-based deep-RIE has an etching mechanism similar to conventional C_4F_8/SF_6 deep-RIE. The etch depth of a 2-μm-wide trench was approximately 0.6 times that of a 50-μm-wide trench.

3.6 Etching resistance of sidewall passivation film to fluorine gas

Next, we investigated the fluorine etching resistance of sidewall passivation films deposited using CO_2 plasma. For the experiment, we used the XeF_2 gas-phase etching process shown in Fig. 9(a).[20] This process allows Si to be etched using gaseous fluorine without using plasma. The etching profile is isotropic. First, we fabricated a line-and-space trench pattern by CO_2/SF_6-based deep-RIE [Fig. 9(b)]. XeF_2 vapor-phase etching was performed at a process pressure of 400 Pa for 5 min. As shown in Fig. 4(b), side etching occurred at the top of the pattern owing to the lack of a passivation film. Next, we etched this sample using XeF_2 gas. As a result, Si, except for the area covered by the passivation film, was isotropically etched, resulting in the profile shown in Fig. 9(c). This indicates that the sidewall passivation film deposited using CO_2 plasma can protect against fluorine etching. Therefore, it was found that the presence of this passivation film makes it possible to achieve the vertical etching of Si through CO_2/SF_6-based deep-RIE.

3.7 Optical emission spectroscopy of deep-RIE plasma

Figures 10(a) and 10(b) show the results of the optical emission spectroscopy of plasma during deep-RIE. A spectrometer (USB4000XR, Ocean Photonics) and an optical fiber were used for the measurements. The measurements were performed through a window above the RF

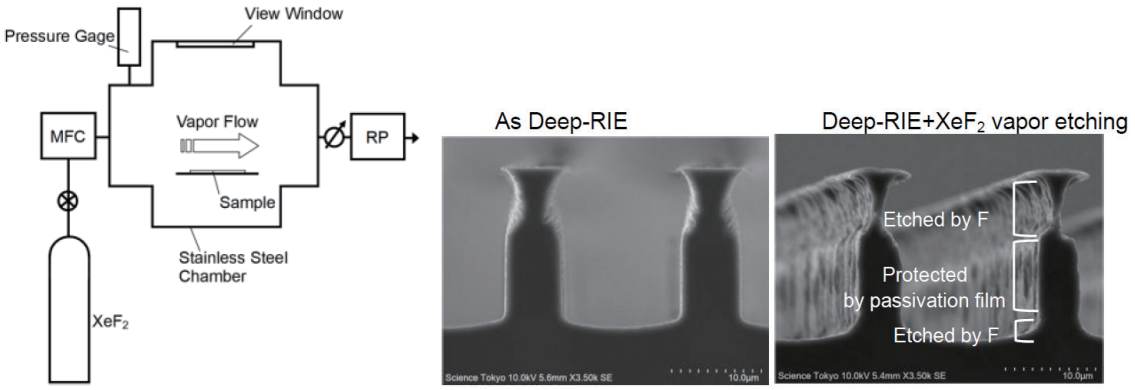

(a) (b) (c)

Fig. 9. (a) XeF_2 vapor-phase etching system, (b) line-and-space trench pattern fabricated by CO_2/SF_6-based deep-RIE, and (c) etching profile obtained after XeF_2 vapor-phase etching.

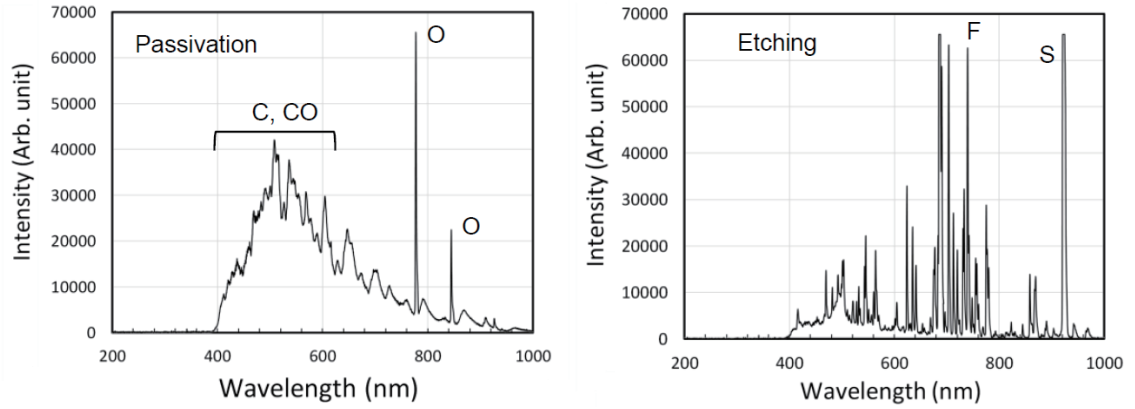

(a) (b)

Fig. 10. Optical emission spectroscopy of plasma during deep-RIE. (a) Passivation process with CO_2. (b) Etching process with SF_6.

coil. This window cuts UV light, so light with wavelengths below 400 nm was not measured. The discharge conditions were a CO_2 flow rate of 880 sccm, an ICP/bias power of 1800/0 W, and a process pressure of 2 Pa. As shown in Fig. 10(a), emissions[21] from C, O, and CO were observed during the passivation process, suggesting that C contributes to the formation of the passivation film as one of the chemical species. On the other hand, as shown in Fig. 10(b), emissions from F and S were mainly observed during etching.

Next, we carried out the optical emission spectroscopy of the plasma during passivation film deposition through a view window on the side of the process chamber. Figures 11(a) and 11(b) show photographs of passivation plasma (CO_2) and etching plasma (SF_6) viewed through the sapphire view window, respectively. This view window is made of sapphire and can pass ultraviolet light. However, because the view window is located below the sample stage, the plasma on the sample is not directly observed. Figure 11(c) shows the optical emission

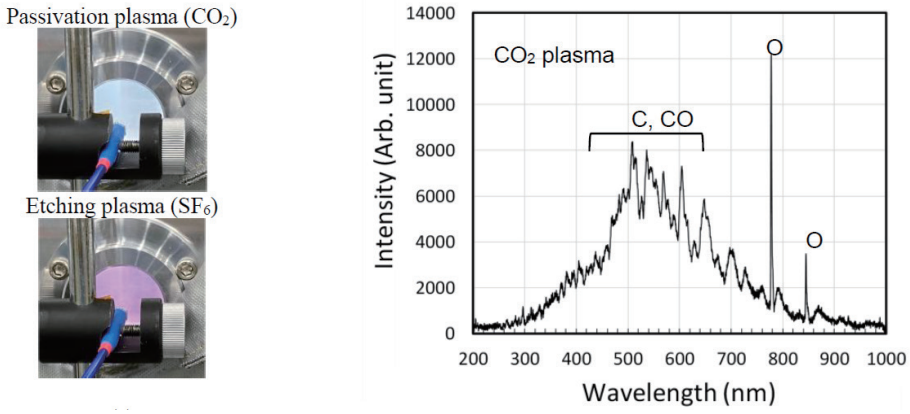

(a) (b)

Fig. 11. (Color online) Photographs of (a) CO_2 plasma and (b) SF_6 plasma observed through a sapphire view window. (c) Optical emission spectrum of the plasma during passivation film deposition.

spectroscopy spectrum of the plasma during passivation film deposition. This spectrum is almost identical to that observed through the window above the RF coil shown in Fig. 10(a), with prominent emissions from C, O, and CO. Because the measurement was performed through the sapphire window, the optical emission spectrum measured also includes wavelengths below 400 nm, compared with the spectrum observed through the window above the RF coil. However, the peak due to the CF_2 species, which appears around 270 nm,[22] is barely observed. Therefore, it is considered that there are many species related to C and O originating from CO_2 in the plasma during the deposition of the passivation film.

3.8 EDX analysis of passivation film

We used a scanning electron miscoscopy system (Flex1000, Hitachi) for EDX analysis. First, a sample with a line-and-space pattern fabricated by deep-RIE [Fig. 4(d)] was cleaved parallel to the pattern to expose the etched sidewall, as shown in Fig. 12(a). Next, EDX was performed by irradiating the etched sidewall with an electron beam perpendicular to it, as shown in Fig. 12(b). Table 1 shows the EDX analysis results for the composition of the passivation film on the etched Si sidewall. The measurement area of the etched sidewall was 15 × 20 μm^2. The electron beam acceleration voltage was 10 kV. This measurement revealed that a large amount of C was deposited on the etched sidewall, which is consistent with our previous results.[19] The amount of F was small, suggesting that C functions as the main component of the passivation film.

3.9 XPS analysis of passivation film

We prepared samples as described above for EDX analysis using an XPS system (Nexsa, Thermo Fisher Scientific). The etching depth (i.e., sidewall height) of the sample was approximately 15 μm. The beam diameter for the XPS analysis was approximately 10 μm. The

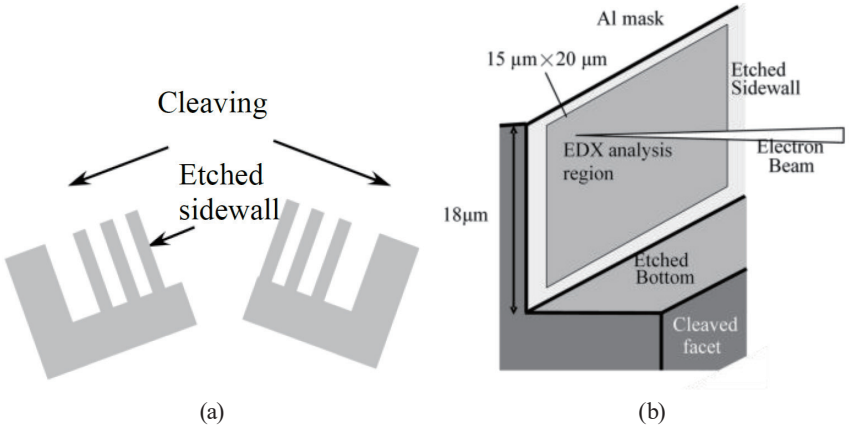

Fig. 12. EDX analysis of the composition of the passivation film on the etched Si sidewall of the sample. (a) Preparation of the analytical surface by cleaving the sample. (b) Measurement area for EDX analysis.

Table 1
Chemical composition of etched sidewall (acceleration voltage: 10 kV).

Atom	Atomic ratio (%)
Si	78.7
C	19.0
O	1.1
F	1.2
S	0.0

beam was irradiated near the center of the sidewall height. Figure 13(a) shows the C1s spectrum. C–C, C–O, and O–C=O bonds were observed. Since the presence of C–F bonds is known to shift the energy to 290 eV,[23] it is considered that C–F bonds are almost absent. Figure 13(b) shows the O1s spectrum. A single peak is observed at 533 eV; this binding energy corresponds to the organic C–O.[24] Figure 13(c) shows the S2p spectrum. A peak is observed near 169 eV. S is characterized by a strong bond, which may be metal sulfate.[25] Figure 13(d) shows the F1s spectrum. A peak can be seen near 689 eV. This may be organic fluorine, which is considered to have a peak at 688–689 eV.[26] Figure 13(e) shows the Si2p spectrum. Si peaks can be seen near 99 and 100 eV, and a SiOx peak can be seen near 103 eV.

Table 2 shows the atomic ratios measured by the XPS analysis of the etched side surfaces of line-and-space trench patterns fabricated by CO_2/SF_6-based deep-RIE. These results also show that the composition of the sidewall passivation film produced by CO_2/SF_6-based deep-RIE contains little F and a lot of C, O, and Si oxides originating from the CO_2 plasma. We consider that the S and F originating from the SF_6 plasma were incorporated into the passivation film when CO_2 and SF_6 were mixed during the switchover between the passivation and etching processes.

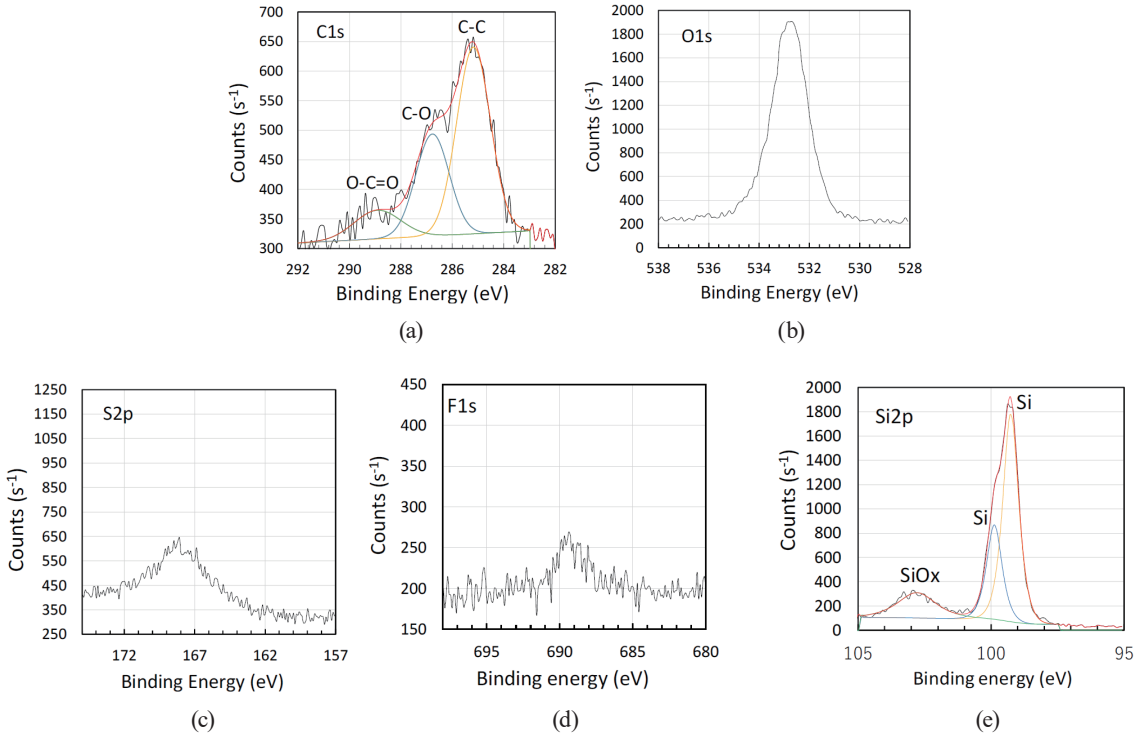

Fig. 13. (Color online) XPS analysis results of the passivation film.

Table 2
Atomic ratio of the etched sidewall of the trench pattern fabricated by CO_2/SF_6-based deep-RIE as measured by XPS analysis.

Atom	Atomic ratio (%)
Si2p	46.72
C1s	17.73
O1s	24.05
F1s	1.36
S2p	10.15

4. Conclusions

In this study, we demonstrated the vertical etching of Si using a CO_2/SF_6-based deep-RIE system. We used CO_2, which has a GWP of 1, as the passivation process gas, instead of C_4F_8, a gas commonly used in deep-RIE. We investigated the dependence of the etching profile on the passivation process time, CO_2 flow rate, ICP power, and process pressure. Furthermore, we performed the optical emission spectroscopy of the plasma during the deep-RIE and EDX and XPS analyses of the chemical composition of the passivation film on the etched Si sidewalls. We found that the main components of the sidewall passivation film in CO_2/SF_6-based deep-RIE are C and O derived from the CO_2 plasma and Si oxides.

The passivation process using CO_2 gas is longer than that using C_4F_8 gas. The deposition rate of the passivation film also depends on factors such as the process pressure and ICP power. For example, when the process pressure is 5 Pa, the deposition rate is 31 nm/min, which is 17% higher than when the process pressure is 2 Pa. Therefore, the process time required to form a passivation film of the required thickness can be reduced by the increase in deposition rate. By optimizing the overall process conditions, taking other conditions into account, the efficiency of the deposition and etching processes could be further improved.

We believe that CO_2/SF_6-based deep-RIE is a highly suitable technique for Si vertical microfabrication.

Acknowledgments

The XPS measurements were performed at the Nagaoka University of Technology, Analysis and Instrumentation Center. We sincerely thank M. Kondo and Y. Ueno of the center for integrated technology support.

References

1 H. Toshiyoshi, M. Mita, and H. Fujita: J. Microelectromech. Syst. **11** (2002) 648. https://doi.org/10.1109/JMEMS.2002.805054
2 M. Esashi and T. Ono: J. Phys. D **38** (2005) R223. https://doi.org/10.1088/0022-3727/38/13/R01
3 B. Wu, A. Kumar, and S. Pamarthy: J. Appl. Phys. **108** (2010) 051101. https://doi.org/10.1063/1.3474652
4 H. V. Jansen, M. J. Boer, S. Unnikrishnan, M. C. Louwerse, and M. C. Elwenspoek: J. Micromech. Microeng. **19** (2009) 033001. https://doi.org/10.1088/0960-1317/19/3/033001
5 C. J. Craigie, T. Sheehan, V. N. Johnson, S. L. Burkett, A. J. Moll, and W. B. Knowlton: J. Vac. Sci. Technol. B **20** (2002) 2229. https://doi.org/10.1116/1.1515910
6 K. J. Morton, G. Nieberg, S. Bai, and S. Y. Chou: Nanotechnology **19** (2008) 345301. https://doi.org/10.1088/0957-4484/19/34/345301
7 A. A. Ayón, R. L. Bayt, and K. S. Breuer: Smart Mater. Struct. **10** (2001) 1135. https://doi.org/10.1088/0964-1726/10/6/302
8 L. Haobing and F. Chollet: J. Microelectromech. Syst. **15** (2006) 541. https://doi.org/10.1109/JMEMS.2006.876660
9 M. Esashi: J. Micromech. Microeng. **18** (2008) 073001. https://doi.org/10.1088/0960-1317/18/7/073001
10 T. Arakawa, H. Kusakawa, and S. Shoji: Proc. 20th IEEE Int. Conf. Micro Electro Mechanical Systems (MEMS 2007), 287. https://doi.org/10.1109/MEMSYS.2007.4433061
11 M. Mizuhata, T. Miyake, Y. Nomoto, and S. Deki: Microelectron. Eng. **85** (2008) 355. https://doi.org/10.1016/j.mee.2007.07.006
12 K.S. Chen, A. A. Ayon, X. Zhang, and S. M. Spearing: J. Microelectromech. Syst. **11** (2002) 264. https://doi.org/10.1109/JMEMS.2002.1007405
13 M. J. de Boer, J. G. E. Gardeniers, H. V. Jansen, E. Smulders, M. J. Gilde, G. Roelofs, J. N. Sasserath, and M. Elwenspoek: J. Microelectromech. Syst. **11** (2002) 385. https://doi.org/10.1109/JMEMS.2002.800928
14 W. T. Pike, W. J. Karl, S. Kumar, S. Vijendran, and T. Semple: Microelectron. Eng. **73**–**74** (2004) 340. https://doi.org/10.1016/j.mee.2004.02.064
15 H. C. Liu, Y. H. Lin, and W. Hsu: Microsyst. Technol. **10** (2003) 29. https://doi.org/10.1007/s00542-003-0309-8
16 C. K. Kang, S. M. Lee, I. D. Jung, P. G. Jung, S. J. Hwang, and J. S. Ko: J. Micromech. Microeng. **18** (2008) 075007. https://doi.org/10.1088/0960-1317/18/7/075007
17 J. H. Min, G. R. Lee, J. K. Lee, S. H. Moon, and C. K. Kim: J. Vac. Sci.Technol. A **22** (2004) 661. https://doi.org/10.1116/1.1722680
18 A. A. Ayón, R. Braff, C. C. Lin, H. H. Sawin, and M. A. Schmidt: J. Electrochem. Soc. **146** (1999) 339. https://doi.org/10.1149/1.1391611
19 A. Matsutani, K. Nishioka, and M. Sato: Jpn. J. Appl. Phys. **55** (2016) 06GH05. https://doi.org/10.7567/JJAP.55.06GH05

20 A. Matsutani, M. Sato, K. Hasebe, and A. Takada: Sens. Mater. **31** (2019) 1325. https://doi.org/10.18494/SAM.2019.2235
21 Z. Li, X. Gillon, M. Diallo, L. Houssiau, J. J. Pireaux: J. Phys. Conf. Series **275** (2011) 012020. https://doi.org/10.1088/1742-6596/275/1/012020
22 Y. Suda, A. Okita, J. Takayama, A. Oda, H. Sugawara, Y. Sakai, S. Oke, and H. Takikawa: IEEE Trans. Plasma Sci. **37** (2009) 1150. https://doi.org/10.1109/TPS.2009.2015451
23 C. B. Labelle, V. M. Donnelly, G. R. Bogart, R. L. Opila, and A. Kornblit: J. Vac. Sci. Technol. **A22** (2004) 2500. https://doi.org/10.1116/1.1810165
24 https://www.thermofisher.com/jp/ja/home/materials-science/learning-center/periodic-table/non-metal/oxygen.html (accessed Dec. 2025).
25 https://www.thermofisher.com/jp/ja/home/materials-science/learning-center/periodic-table/non-metal/sulfur.html (accessed Dec. 2025).
26 https://www.thermofisher.com/jp/ja/home/materials-science/learning-center/periodic-table/halogen/fluorine.html (accessed Dec. 2025).